Supporting Information

Efficient construction of high-quality sulfonated porous aromatic frameworks by optimizing swelling state of porous structure

Lulu Yang‡[a], Zhen Zhan‡[b], Lin Zhao[a], Chengxin Zhang[a,c], Shaolei Wang[a*], Wei Hu[a*], Guangshan Zhu[a*]

[a] Key Laboratory of Polyoxometalate and Reticular Material Chemistry of Ministry of Education, Faculty of Chemistry, Northeast Normal University, Changchun, 130024, China.

[b] Department of Applied Physics, The Hong Kong Polytechnic University, Kowloon, 999077, Hong Kong SAR, China

[c] School of Materials Science and Engineering, Shenyang Ligong University, Shenyang, 110159, China.

Table of Contents

Materials and Methods

Chemicals and Reagents:

Hydrochloric acid, Sodium hydroxide, anhydrous ferric chloride, 1, 2-dichloroethane (DCE) and divinylbenzene (DVB) were purchased from Shanghai Aladdin Biochemical Technology Co., Ltd. Chlorosulfonic acid ($ClSO_3H$) and Ciprofloxacin (CIP) were purchased from AnhAui Zesheng Technology Co., Ltd. Methylene Blue (MB), Rhodamine B (RhB) and Tetracycline (TC) were purchased from Shanghai Macklin Biochemical Co., Ltd. All the reagents are of analytical grade and used as received.

Synthesis of sulfonated KAP-1 (one-pot method):

1.22 g anhydrous $FeCl_3$ (7.5 mmol) is added into the solution of 0.195 g benzene (2.5 mmol), 0.57 g formaldehyde dimethyl acetal (FDA, 7.5 mmol) and 10 mL DCE. The mixture is firstly stirred at 45 ^oC for 5 h, and then heated at 80 ^oC for 19 h. The reaction system is further cooled to room temperature, and then 20 mL DCE and 15 mL $ClSO_3H$ are sequentially added into the reaction system under an ice water bath, followed by stirring at room temperature for 1 d. Finally, the post-sulfonation reaction is quenched in ice water, and the sulfonated KAP-1 is washed by distilled water to neutral, extracted with methanol by soxhlet for 2 d, and then dried under vacuum at 60 ^oC.

Synthesis of KAP-1 and sulfonated KAP-1 (conventional post-sulfonation method):

1.22 g anhydrous $FeCl_3$ (7.5 mmol) is added into the solution of benzene (0.195 g, 2.5 mmol), FDA (0.57 g, 7.5 mmol) and 10 mL DCE. The mixture is firstly stirred at 45 ^oC for 5 h, and then heated at 80 ^oC for 19 h. The resulting precipitate is washed three times with methanol, and then extracted with methanol by soxhlet for 24 h, and then dried under vacuum at 60 ^oC for 24 h to obtain KAP-1. Subsequently, 0.2 g KAP-1 and 12 mL DCE are added into 25 mL round bottom flask to thoroughly swell polymer framework for 2 d. 6 mL $ClSO_3H$ is added into the reaction system under an ice water bath, followed by stirring at room temperature for 1 d to complete sulfonation. Finally, the post-sulfonation reaction is quenched in ice water, and the sulfonated KAP-1 is washed by distilled water to neutral, extracted with methanol by soxhlet for 2 d, and then dried under vacuum at 60 ^oC.

Synthesis of sulfonated CMP-1 (improved post-sulfonation method):

The CMP-1 is prepared by employing the reported method.[1] The CMP-1 after purification is extracted with DCE by soxhlet to replace original solvents of porous structure. After multiple solvent extractions, 0.2 g CMP-1 and 30 mL DCE are added into 100 mL round bottom flask, and then 15 mL $ClSO_3H$ is dropwise added into the reaction system under an ice water bath, followed by stirring at room temperature for 1 d. Finally, the post-sulfonation reaction is quenched in ice water, and the sulfonated CMP-1 is washed by distilled water to neutral, extracted with

methanol by soxhlet for 2 d, and then dried under vacuum at 60 °C.

Synthesis of sulfonated CMP-1 (conventional post-sulfonation method):

The CMP-1 is prepared by employing the reported method.[1] Subsequently, 0.2 g CMP-1 and 30 mL DCE are added into 100 mL round bottom flask to thoroughly swell porous framework for 2 d. 15 mL $ClSO_3H$ is dropwise added into the reaction system under an ice water bath, followed by stirring at room temperature for 1 d. Finally, the post-sulfonation reaction is quenched in ice water, and the sulfonated CMP-1 is washed by distilled water to neutral, extracted with methanol by soxhlet for 2 d, and then dried under vacuum at 60 °C.

Characterization:

Fourier transform infrared spectroscopy (FT-IR) was measured with KBr pellets via NICOLET iS50. ^{13}C Solid-state NMR was measured on a BRUKER AVANCE NEO 400WB NMR spectrometer. The nitrogen adsorption-desorption isotherms were measured on a Quantachrome Autosorb iQ at 77.3 K, and the pore size distribution (PSD) was obtained according to the NLDFT calculation model. Thermo-gravimetric analysis (TGA) was measured on TGA/DSC 3^+ thermalanalyzer in the temperature range of 30-800 ℃ with a heating rate of 10 ℃ min^{-1} under N_2 atmosphere and air atmosphere, respectively. Field emission scanning electron microscopic analysis (FE-SEM) was performed on a HITACHI SU8010 microscope. Sulfur content was measured through Elementar UNICUBE. Water vapor adsorption and desorption isotherms were measured on QuantachromeVstar4 vapor sorption analyzer at 298K from 0 to 1 bar relative pressure. The UV-Vis absorption spectroscopy was measured through the Agilent VARIAN Cary-60 UV-Vis spectrophotometer in the wavelength range of 200-800 nm.

Adsorption kinetics:

MB, RhB, CIP and TC were selected as the micro-pollutant models for adsorption experiments at room temperature (298 K) (Note: CIP and TC aqueous solution need avoid light). All the porous adsorbents were ground in agate mortar before use. Then an UV-vis spectrophotometer was used to measure the concentration of different pollutants in water. The detection wavelengths of MB, RhB, CIP and TC are 664, 553, 277 and 355 nm, respectively. All reported experimental data are the average values of three parallel experiments.

40 mg adsorbent was added to a 50 mL micro-pollutant solution (200 ppm MB and RhB solution, 180 ppm CIP and TC solution) and stirred immediately. The residual concentration of the pollutant in each sample was determined by UV–vis spectroscopy. At certain intervals about 700 μL of the suspension was withdrawn and filtered immediately through a Whatman 0.45 μm inorganic membrane. After the filtration process, the residual concentration of the pollutant was analyzed by an UV-visible spectrophotometer.

The micro-pollutants removal efficiency was calculated by following equation:

$$\textbf{Removal efficiency}\ (\%) = \frac{(c_0 - c_t)}{c_0} \times 100 \quad \text{S1}$$

where c_0 (mg L^{-1}) and c_t (mg L^{-1}) are representing the initial and residual concentration of contaminants in the filtrate at certain time, respectively.

The adsorption capacity in equilibrium q_e (mg g^{-1}) is calculated by equation followed:

$$q_e = \frac{(c_0 - c_e)}{m} \times V \quad \text{S2}$$

Where c_0 and c_e (mg L^{-1}) meant initial concentration and final concentrations of micro-pollutants, V (mL) is the volume of the micro-pollutions aqueous solutions, and m (mg) meant the adsorbents mass.

The adsorption rate was approximately described by linear pseudo-first-order and pseudo-second-order adsorption models with the following equations (S3) and (S4), respectively:

$$\log (q_e - q_t) = \log q_e - \frac{k_1}{2.303} t \quad \text{S3}$$

$$\frac{t}{q_t} = \frac{1}{K_2 q_e^2} + \frac{1}{q_e} t \quad \text{S4}$$

Where q_t and q_e are the adsorption amounts of pollutants (mg g^{-1}) at time t (min) and at equilibrium respectively, k_1(min^{-1}) and k_2 (g mg^{-1} min^{-1}) are the pseudo-first and second-order rate constants.

Adsorption isotherms:

3 mg of adsorbent was added to 18 mL micro-pollutant solution (0-500 ppm for MB and RhB, 0-300 ppm for CIP, 0-400 ppm for TC). Each suspension was stirred 1 h to achieve equilibrium. Then the dispersion was filtered through a Whatman 0.45 μm inorganic membrane and the filtered solution was measured by UV-vis absorption spectroscopy.

The Langmuir and Freundlich adsorption models were generated by fitting the adsorption isotherms by the following equations (S5) and (S6), respectively:

$$\frac{c_e}{q_e} = \frac{1}{q_m \times K_L} + \frac{c_e}{q_m} \quad \text{S5}$$

$$\ln q_e = \ln K_F + \frac{1}{n} \ln c_e \quad \text{S6}$$

where q_e (mg g^{-1}) is the equilibrium adsorption amount of pollutant, q_{max} (mg g^{-1}) is the maximum adsorption capacity of adsorbent at equilibrium, c_e (mg L^{-1}) is the remaining pollutant concentration after the adsorption equilibrium, K_L (L mg^{-1}) is the adsorption equilibrium constant, K_F and n are associated with the uptake coefficients of Freundlich.

Influence of pH and temperature:

5 mg PAF-215 was mixed into 40 mL micro-pollutant solutions under different pH value and temperature conditions for 2 h to achieve equilibrium. Then the dispersion was filtered through a Whatman 0.45 μm inorganic membrane and the filtered solution was measured by UV-vis absorption spectroscopy. The pH values of micro-pollutant solutions were tuned by adding 1M HCl or NaOH solutions.

Reusability of PAF-215:

40 mg PAF-215 was added to 50 mL micro-pollutant solutions (200 ppm MB and RhB solution, 180 ppm CIP and TC solution) for 1 h. PAF-215 was collected through vacuum filtration, washed with 1M HCl methanol mixture used as an eluent and dried under vacuum at 60 ℃.

Supporting Figures

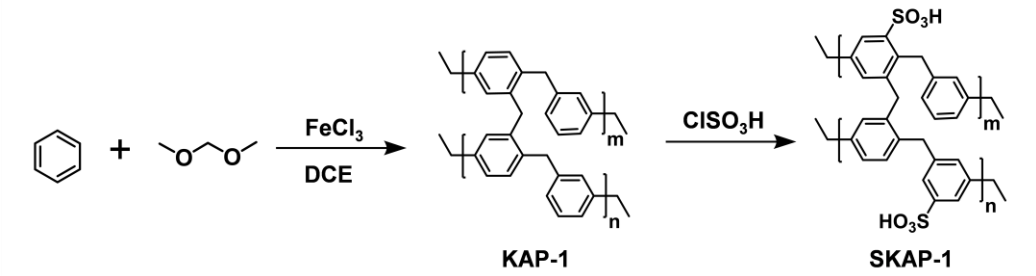

Fig S1. Reaction schemes for synthesis of KAP-1 and SKAP-1.

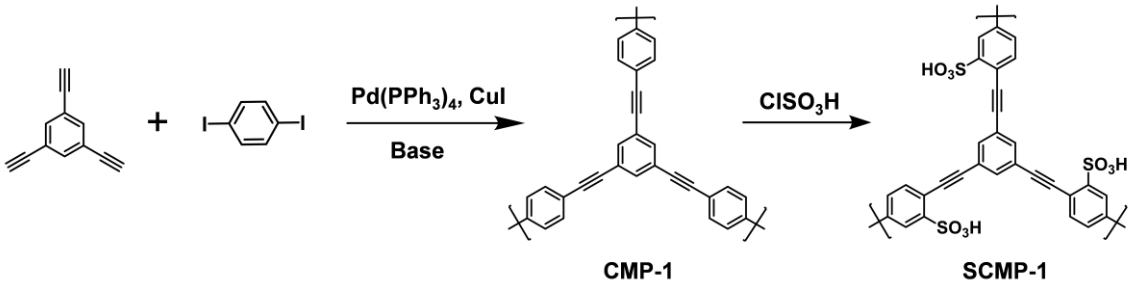

Fig S2. Reaction schemes for synthesis of CMP-1 and SCMP-1.

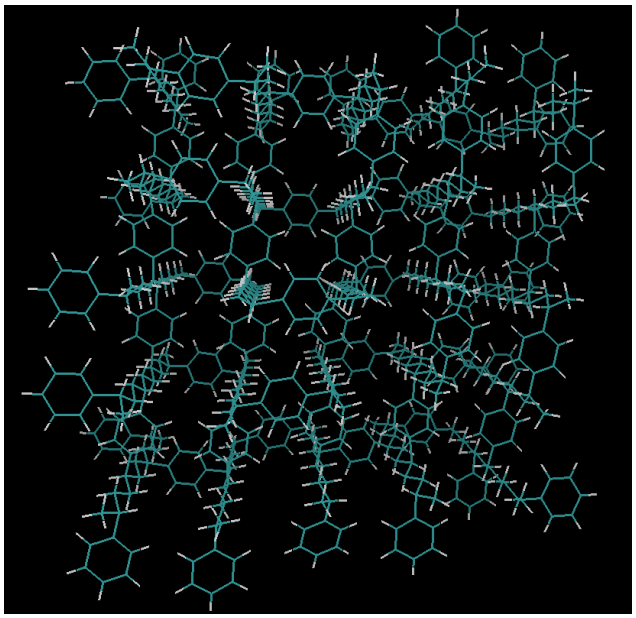

Figure S3. Structure schematic illustration of porous precursor drawn by VMD (Visual Molecular Dynamics) with blue for carbon element, white for hydrogen element, respectively.

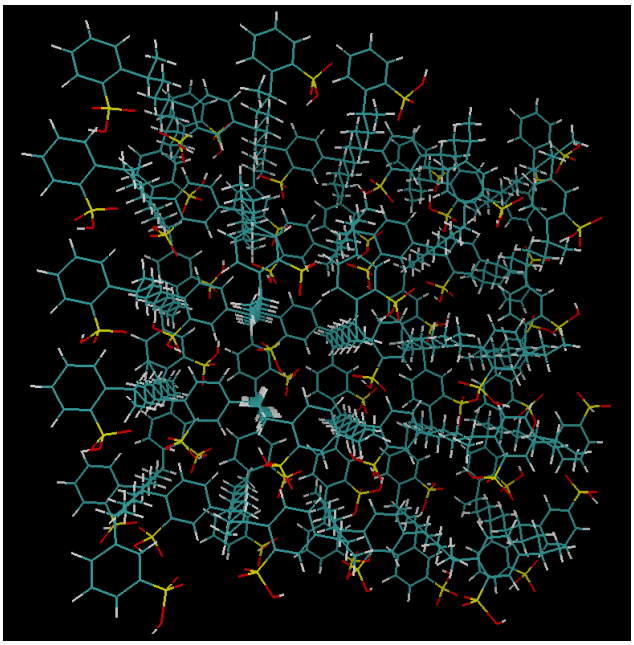

Figure S4. Structure schematic illustration of PAF-215 drawn by VMD (Visual Molecular Dynamics) with blue for carbon element, white for hydrogen element, red for sulfur element and yellow for oxygen element respectively.

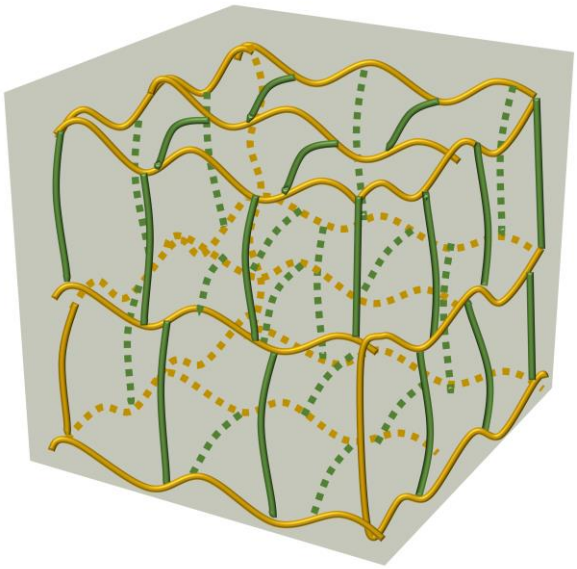

Figure S5. Structure diagram of porous precursor (The yellow line and green line mark polymer chains and phenyl rings respectively).

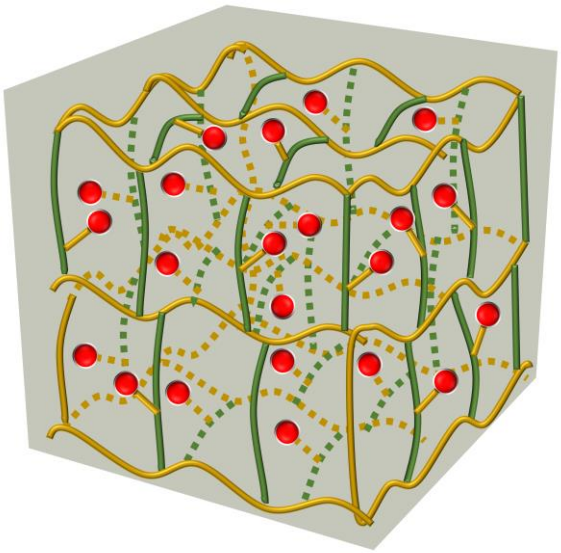

Figure S6. Structure diagram of PAF-215 (The yellow line and green line mark polymer chains and phenyl rings respectively, and red dots represent sulfonic acid groups).

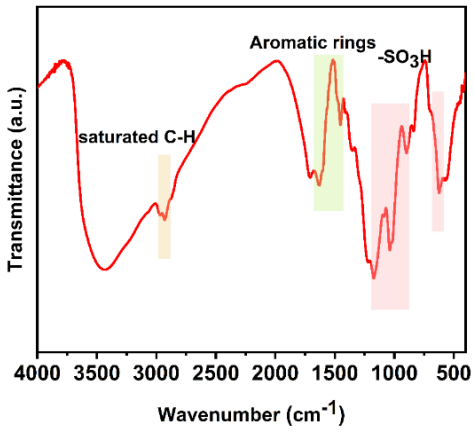

Figure S7. FT-IR spectrum of PAF-215.

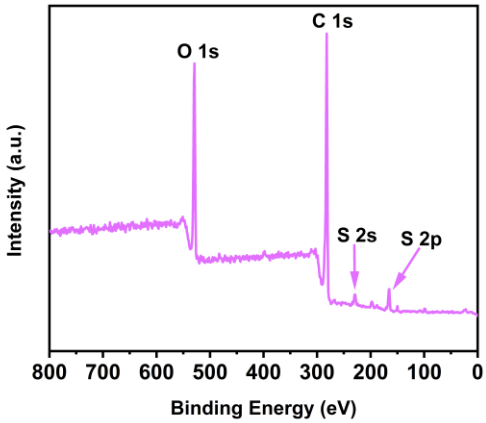

Figure S8. XPS spectrum of PAF-215.

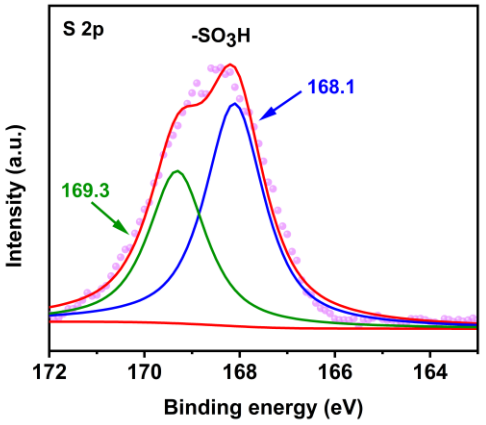

Figure S9. S 2p high resolution XPS spectra of PAF-215.

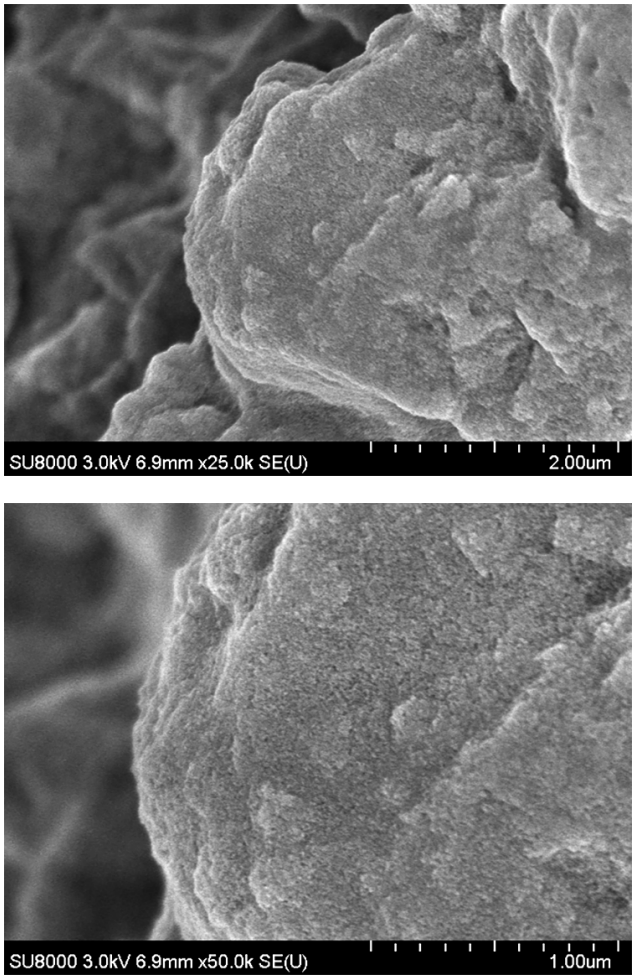

Figure S10. FE-SEM images of PAF-215 at different scale bars (2 μm and 1 μm, respectively).

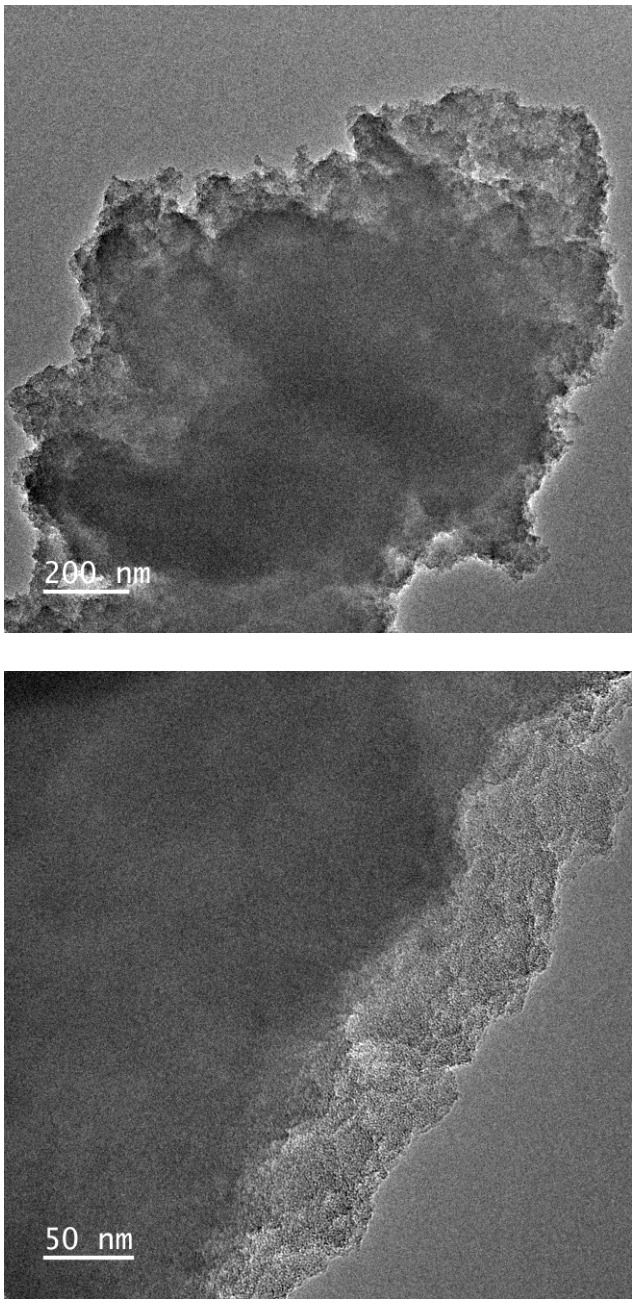

Figure S11. HR-TEM images of PAF-215 at different scale bars (200 nm and 50 nm, respectively).

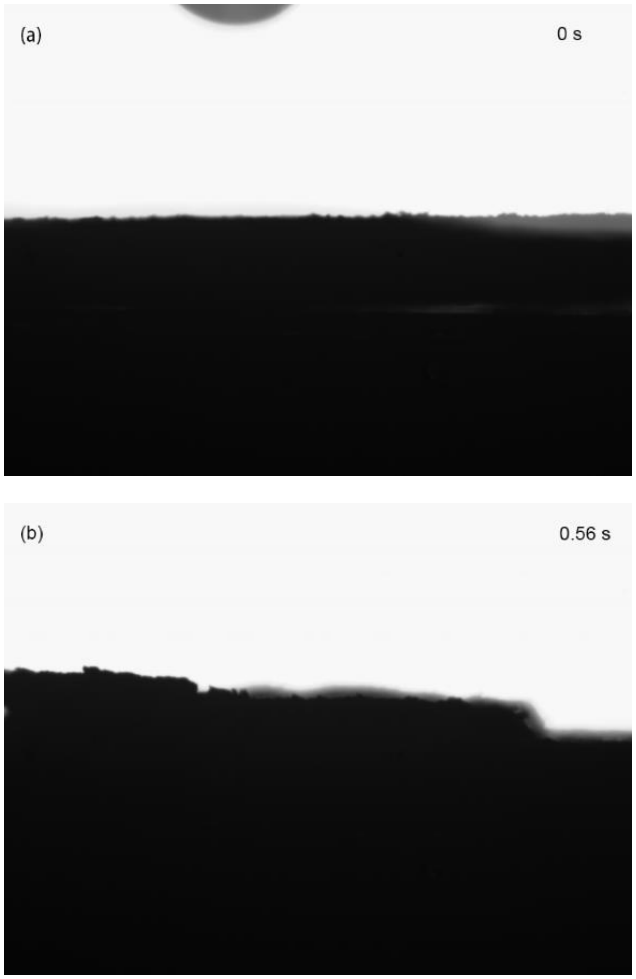

Figure S12. Water contact angle of PAF-215.

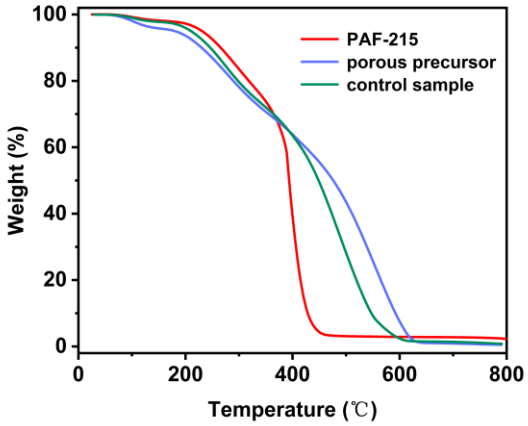

Figure S13. Thermo-gravimetric analysis (TGA) profile of porous precursor, control sample and PAF-215 in air atmosphere.

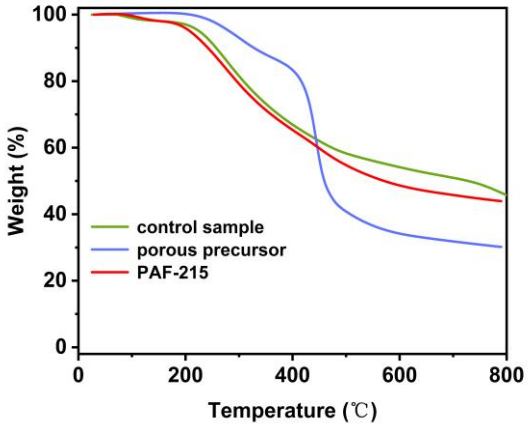

Figure S14. Thermo-gravimetric analysis (TGA) profile of porous precursor, control sample and PAF-215 in nitrogen atmosphere.

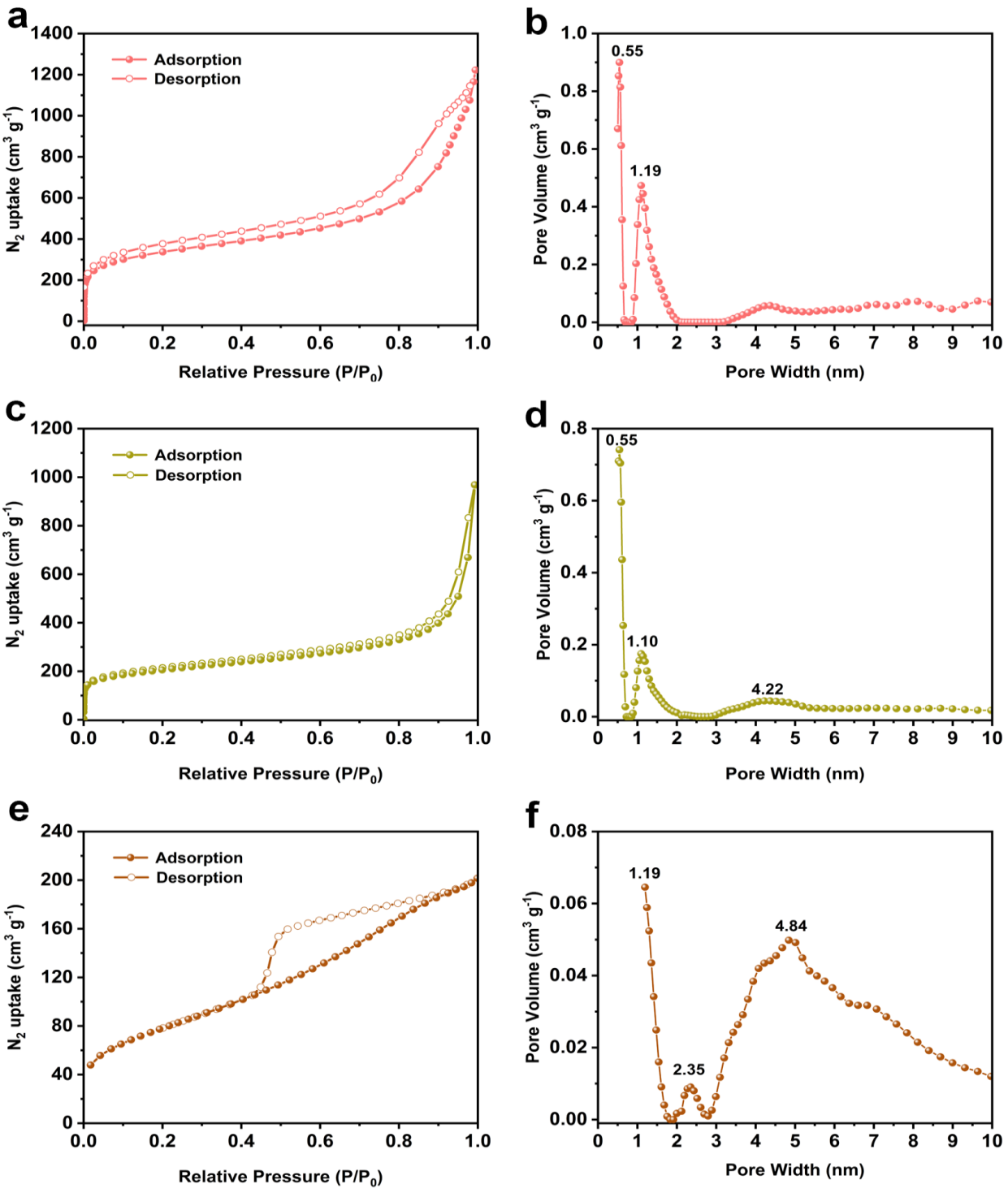

Figure S15. N_2 adsorption and desorption isotherms of (a) KAP-1, (c) sulfonated KAP-1 (one-pot method) and (e) sulfonated KAP-1 (conventional post-sulfonation method) at 77.3 K; Pore size distributions of (b) KAP-1, (d) sulfonated KAP-1 (one-pot method) and (f) sulfonated KAP-1 (conventional post-sulfonation method) calculated by using density functional theory (DFT) methods (slit pore models and differential pore volumes).

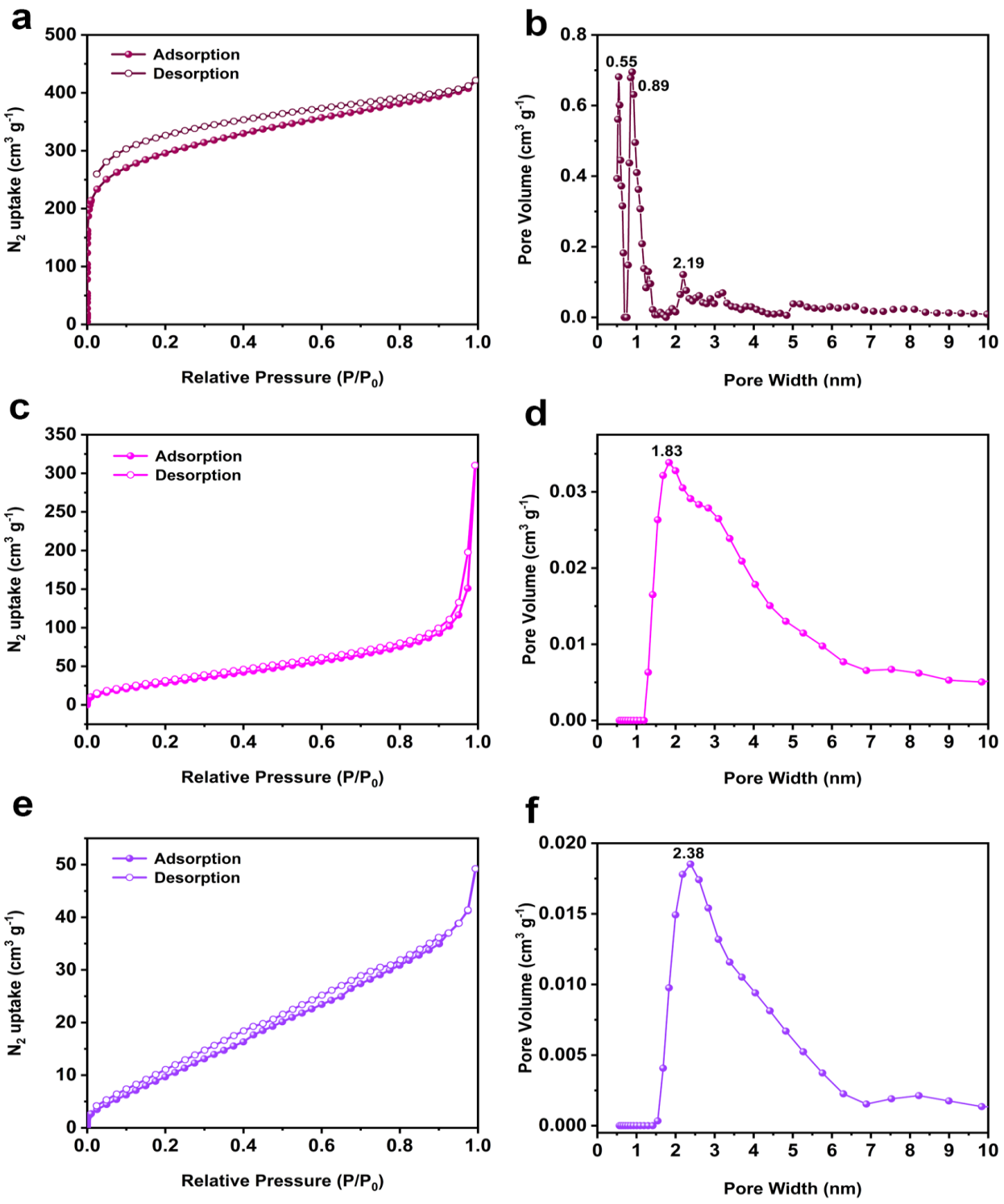

Figure S16. N_2 adsorption and desorption isotherms of (a) CMP-1, (c) sulfonated CMP-1 (improved post-sulfonation method) and (e) sulfonated CMP-1 (conventional post-sulfonation method) at 77.3 K; Pore size distributions of (b) CMP-1, (d) sulfonated CMP-1 (improved post-sulfonation method) and (f) sulfonated CMP-1 (conventional post-sulfonation method) calculated by using density functional theory (DFT) methods (slit pore models and differential pore volumes).

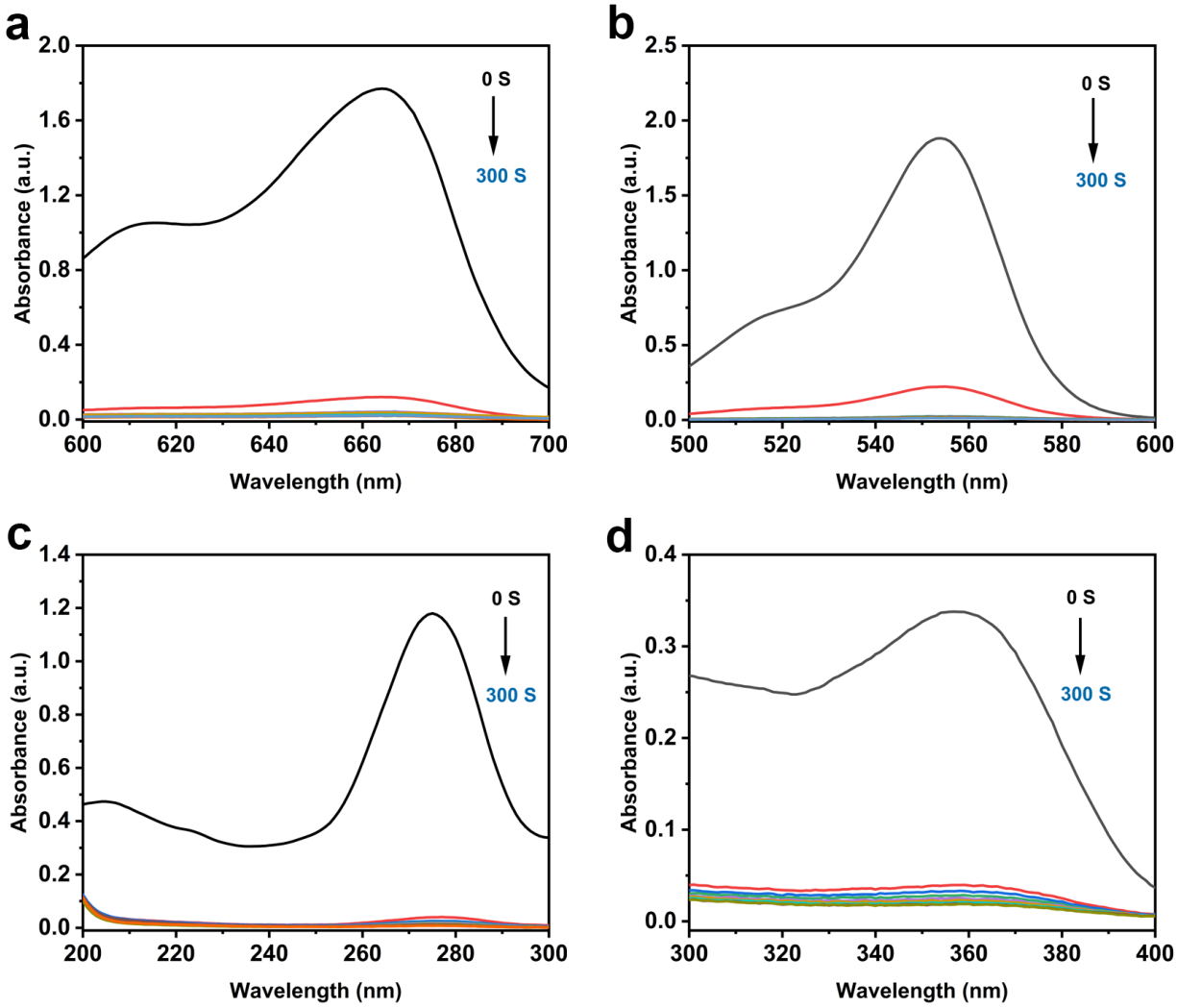

Figure S17. UV–vis absorbance spectra of MB (a), RhB (b), CIP (c) and TC (d) aqueous solution of PAF-215 at 25 ppm.

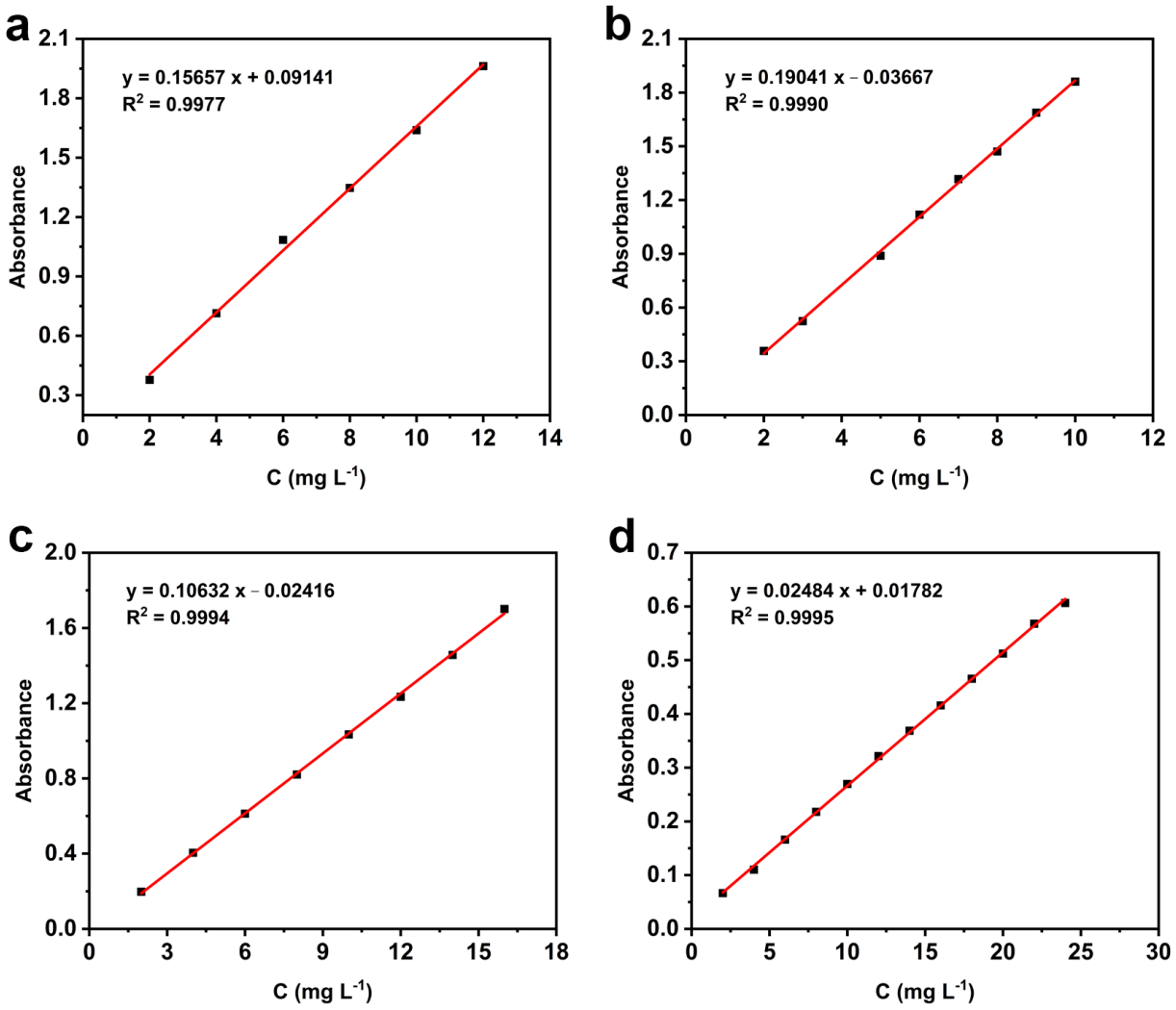

Figure S18. Standard curves of MB (a), RhB (b), CIP (c) and TC (d).

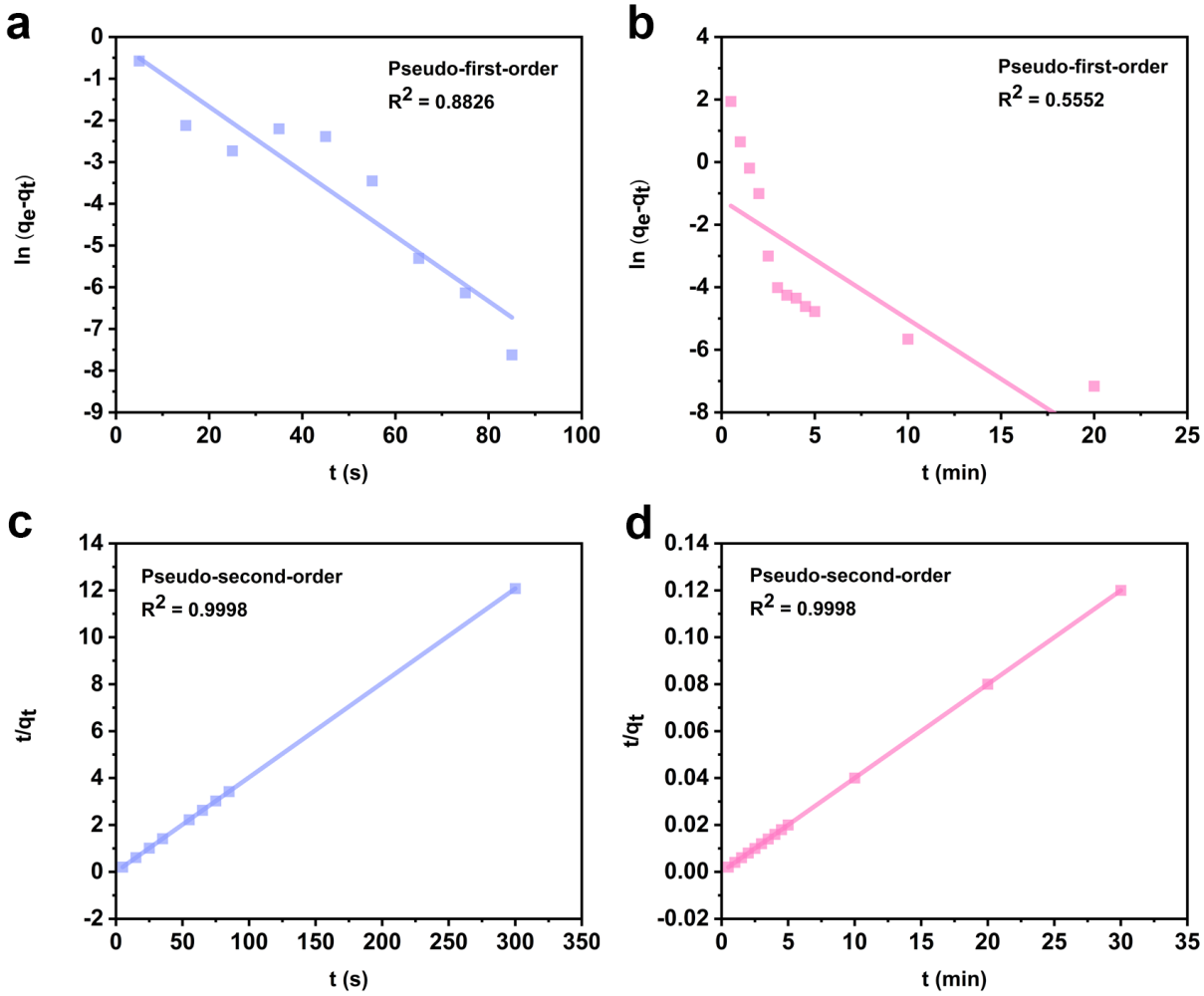

Figure S19. Pseudo-first-order kinetic data of PAF-215 for MB at 25 ppm (a) and 200 ppm (b); Pseudo-second-order kinetic data of PAF-215 for MB at 25 ppm (c) and 200 ppm (d).

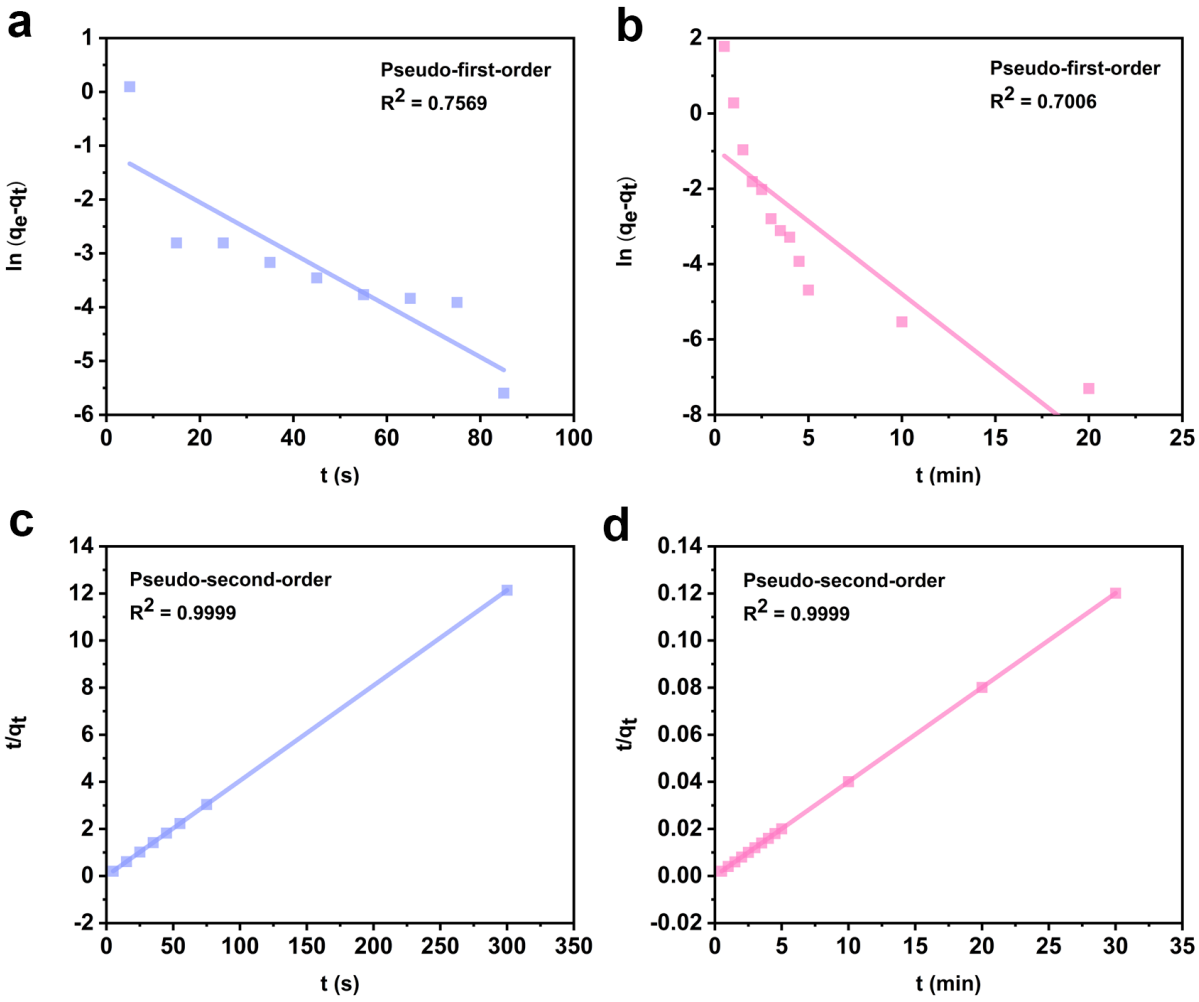

Figure S20. Pseudo-first-order kinetic data of PAF-215 for RhB at 25 ppm (a) and 200 ppm (b); Pseudo-second-order kinetic data of PAF-215 for RhB at 25 ppm (c) and 200 ppm (d).

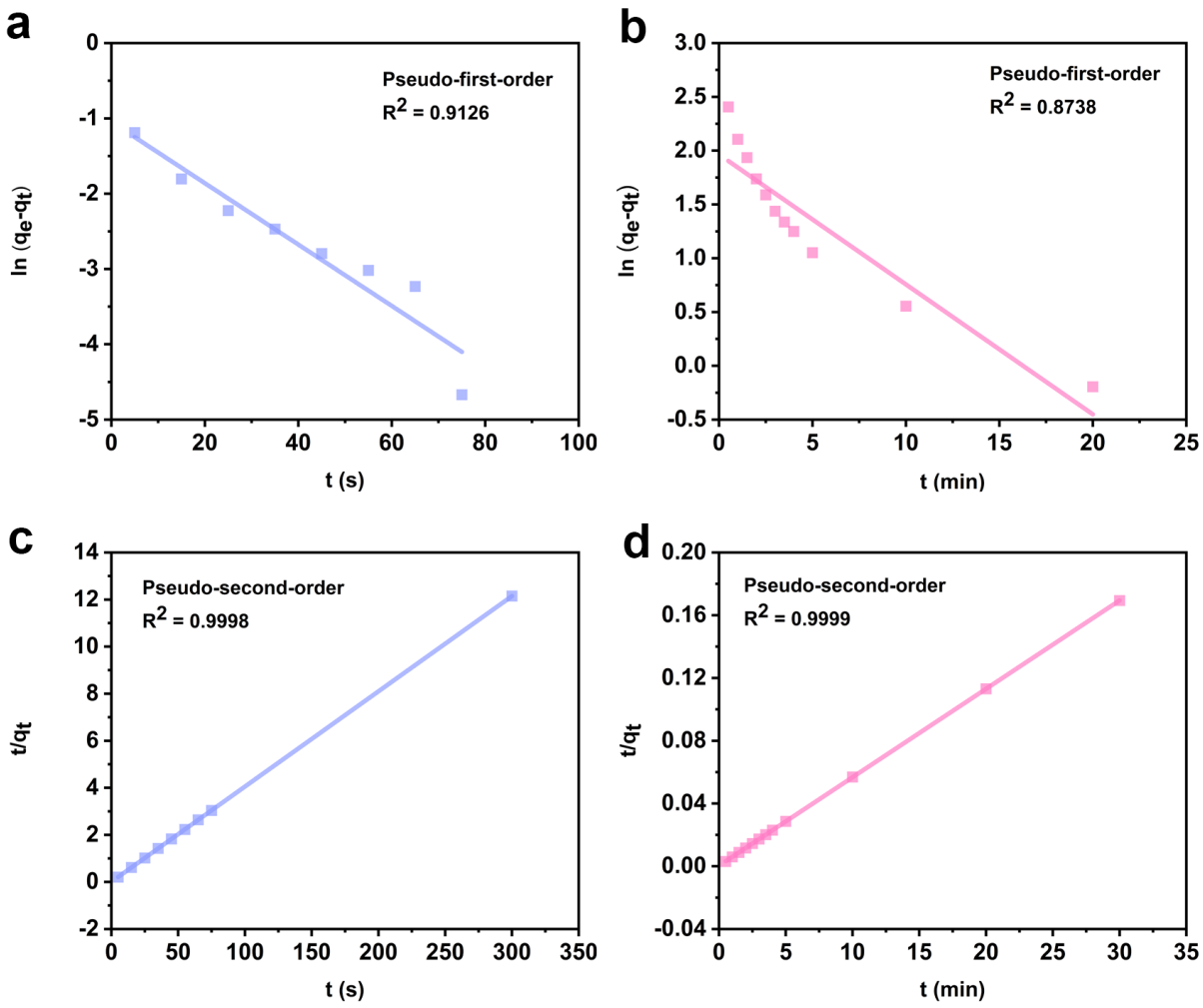

Figure S21. Pseudo-first-order kinetic data of PAF-215 for CIP at 25 ppm (a) and 180 ppm (b); Pseudo-second-order kinetic data of PAF-215 for CIP at 25 ppm (c) and 180 ppm (d).

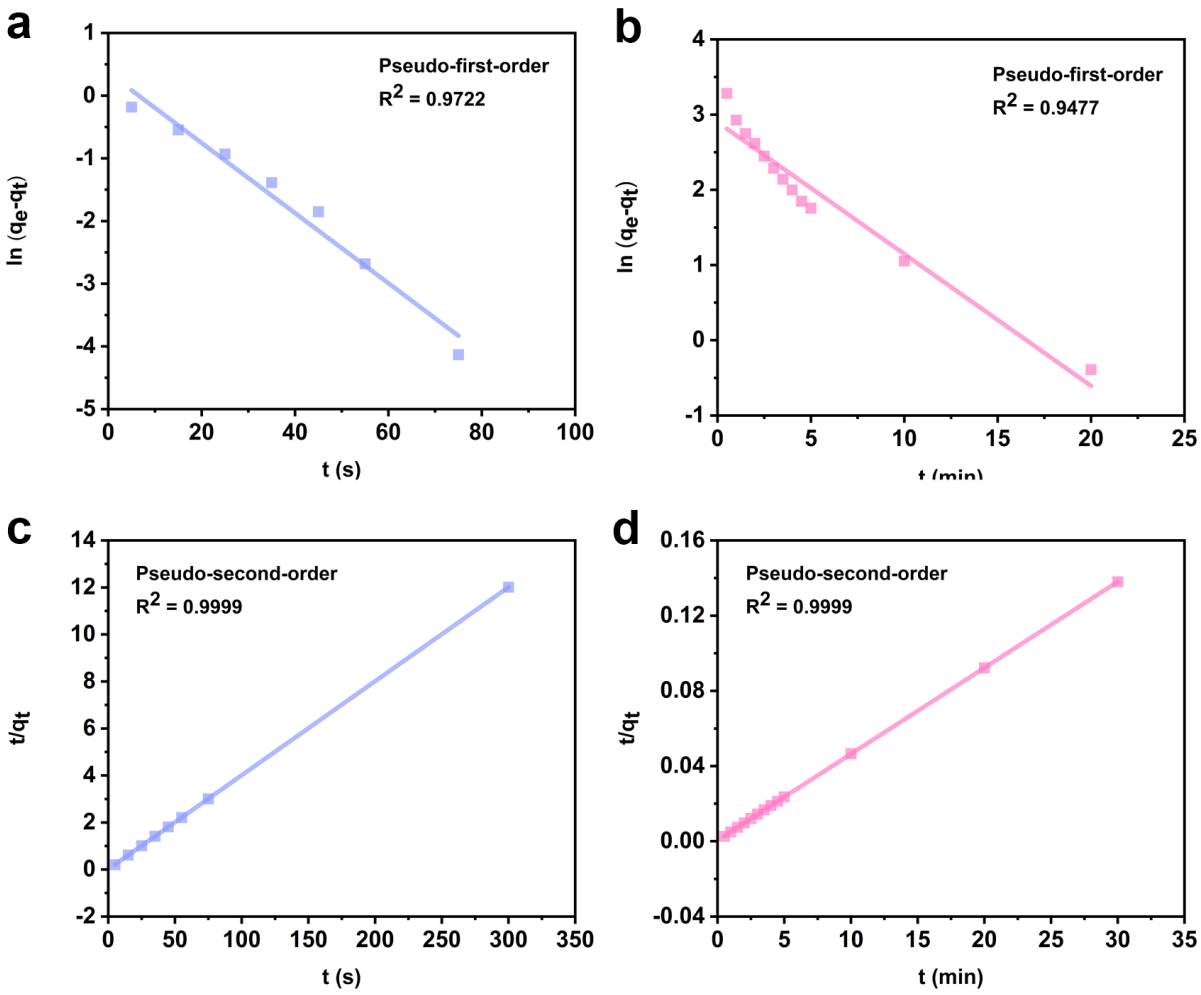

Figure S22. Pseudo-first-order kinetic data of PAF-215 for TC at 25 ppm (a) and 180 ppm (b); Pseudo-second-order kinetic data of PAF-215 for TC at 25 ppm (c) and 180 ppm (d).

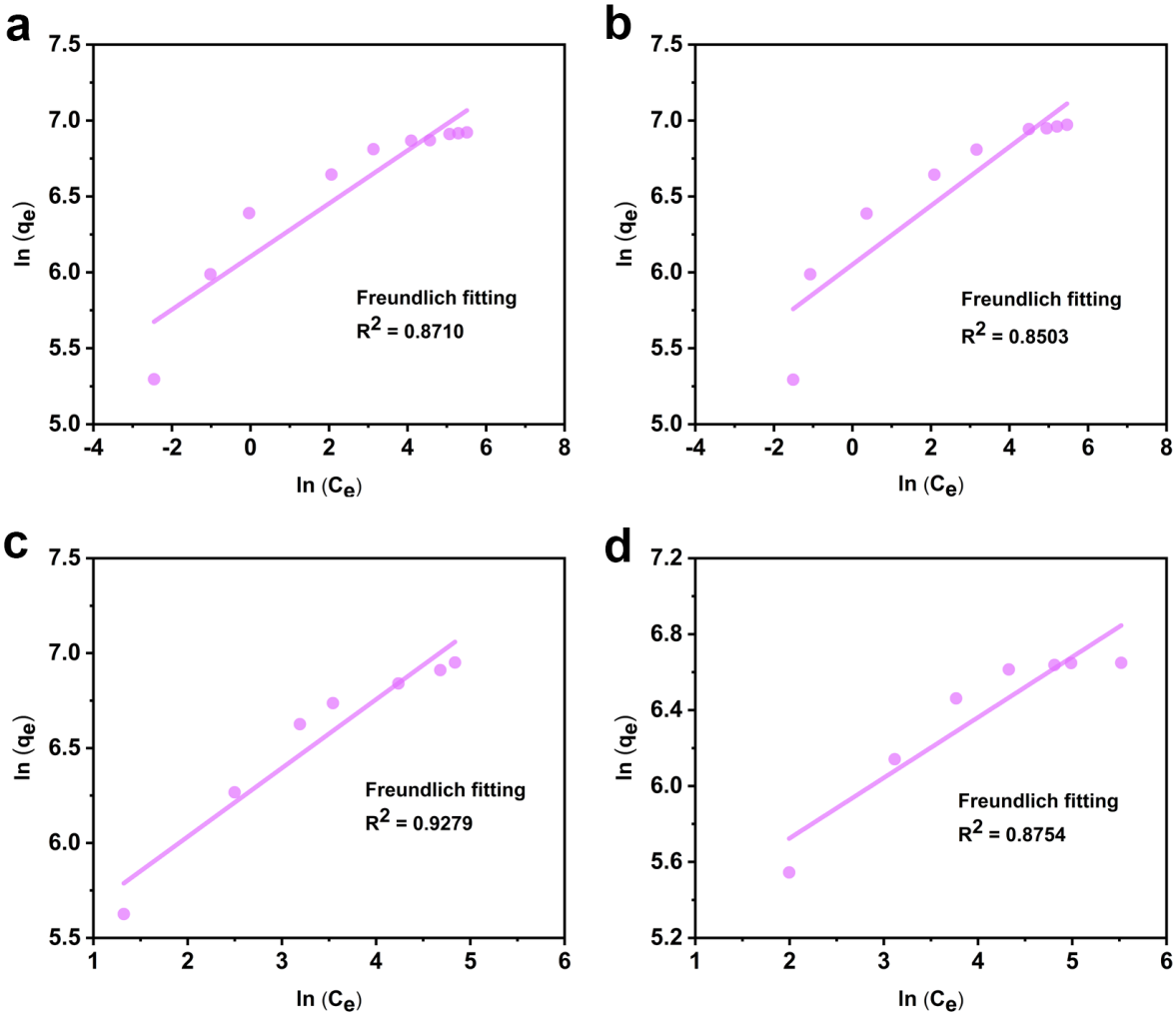

Figure S23. The fitting curves of Freundlich isotherm model for MB (a), RhB (b), CIP (c) and TC (d).

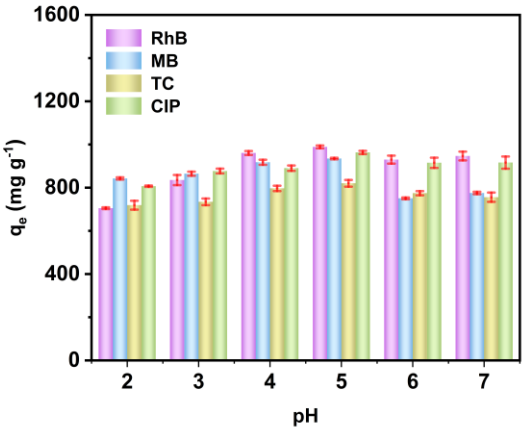

Figure S24. The maximum adsorption capacity of PAF-215 at different pH value.

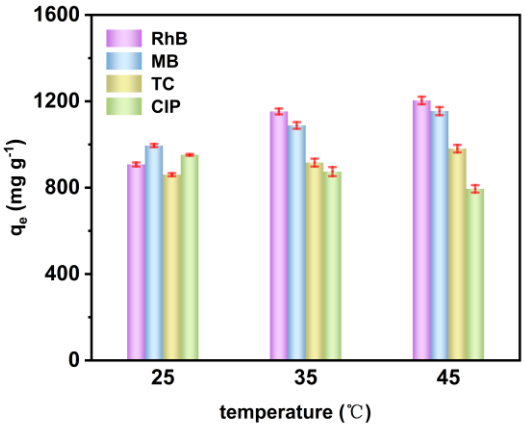

Figure S25. The maximum adsorption capacity of PAF-215 at different temperature.

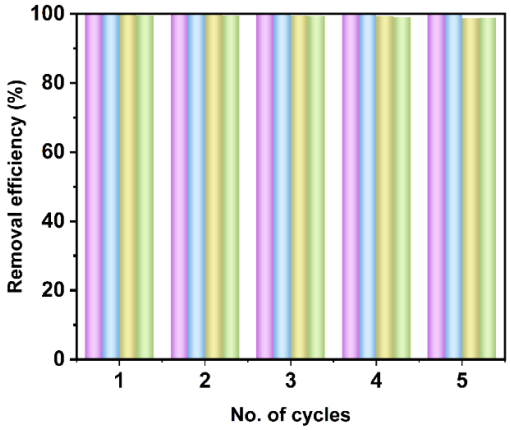

Figure S26. Regeneration performance of PAF-215 for micro-pollutants models MB (blue), RhB (purple), CIP (green) and TC (yellow).

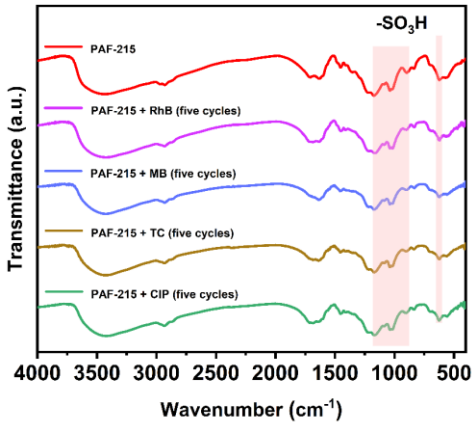

Figure S27. FT-IR spectra of PAF-215 after 5 cycles.

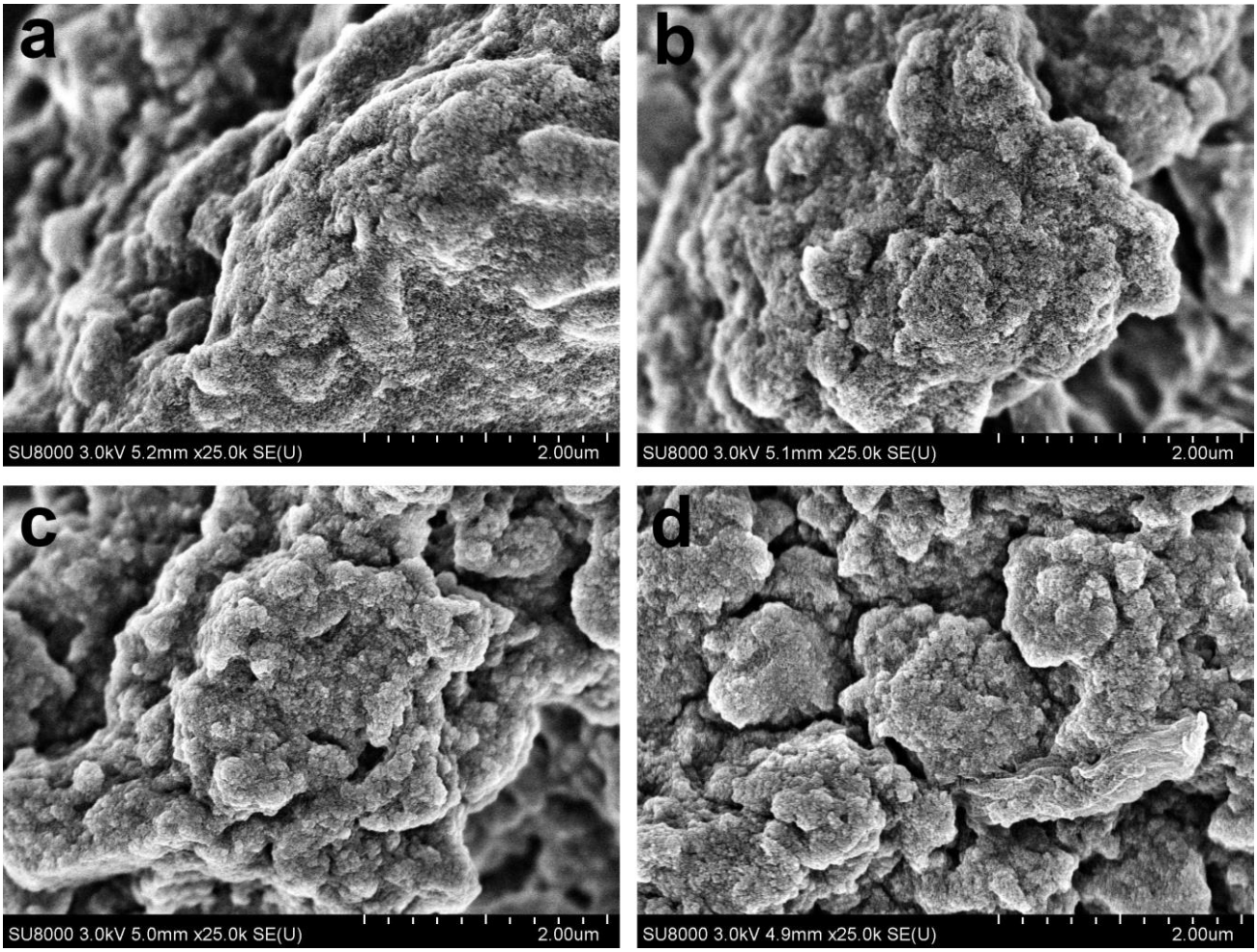

Figure S28. FE-SEM images of PAF-215 after 5 cycles at 2 μm for PAF-215 + RhB (a), PAF-215 + MB (b), PAF-215 + TC (c) and PAF-215 + CIP (d).

Supporting Tables

Table S1. Adsorption rate and equilibrium adsorption capacity of micro-pollutants at 25 ppm.

Micro-pollutants	% uptake at 5s	% uptake at equilibrium	Adsorption capacity of equilibrium（mg g^{-1}）
MB	97.31	99.18	24.79
RhB	94.57	98.85	24.71
CIP	97.58	98.76	24.69
TC	96.57	99.84	24.96

Table S2. Adsorption kinetics data of micro-pollutants at 25 ppm.

Micro-pollutants	Pseudo-first-order model		Pseudo-second-order model	
	K_1 (min^{-1})	R^2	K_2 (g mg^{-1} min^{-1})	R^2
MB	10.74	0.8826	25.39	0.9998
RhB	6.62	0.7569	26.80	0.9999
CIP	5.63	0.9126	22.59	0.9998
TC	7.73	0.9722	9.18	0.9999

Table S3. Kinetics parameters for the removal of different micro-pollutants.

Micro-pollutants	Pseudo-first-order model		Pseudo-second-order model	
	K_1 (min^{-1})	R^2	K_2 (g mg^{-1} min^{-1})	R^2
MB[a]	0.88	0.5552	1.07	0.9998
RhB[a]	0.89	0.7006	1.33	0.9999
CIP[b]	0.28	0.8738	0.08	0.9999
TC[b]	0.40	0.9477	0.04	0.9999

[a)] The concentration of MB and RhB is 200 ppm; [b)] The concentration of MB and RhB is 180 ppm.

Table S4. The k_2 value of PAF-215 and other porous adsorbents.

Micro-pollutants	Adsorbents	k_2 (g mg^{-1} min^{-1})	References
	DMpillar[5]	1.097	[2]
	CaPy	0.000234	[3]
RhB	10% NH_2-ZIF-2 h	0.418	[4]
	POP-T (1:1.5)	0.012	[5]
	PAF-215	26.80	This Work
	CaO-ES@GO	0.00454	[6]
	TzDABA COF	0.017	[7]
MB	CTT-POP-2	1.91	[8]
	Co/C-1000	0.000993	[9]
	PAF-215	25.39	This Work
	Fe-BTC-HBs	0.0002	[10]
	ZIF-67@WA	0.0000758	[11]
TC	CM	0.000078	[12]
	NMF/TT-90	0.000765	[13]
	PAF-215	9.18	This Work
	SMC	0.017	[14]
	COF@MXene	0.0016	[15]
CIP	Tb@TpPa-SO_3H	8.05	[16]
	Fe-POP	0.038	[17]
	PAF-215	22.59	This Work

Table S5. The parameters of different isotherm models for PAF-215.

Micro-pollutants	Langmuir model			Freundlich model		
	q_m[a] (mg g^{-1})	k_L[b] (L mg^{-1})	R^2[c]	K_F[d] (mg g^{-1})	1/n[e]	R^2[f]
RhB	1075	0.45	0.9996	425	0.19	0.8503
MB	1020	0.50	0.9997	448	0.17	0.8710
TC	826	0.075	0.9989	162	0.31	0.8754
CIP	1134	0.079	0.9990	202	0.36	0.9279

[a)] The maximum adsorption capacity calculated by the Langmuir model; [b)] The adsorption capacity constant of the Langmuir model; [c)] The correlation coefficients of the Langmuir model; [d)] The adsorbent capacity constant of the Freundlich model; [e)] The n is the heterogeneity factor and $1/n$ is the adsorption intensity of the Freundlich model; [f)] The correlation coefficients of the Freundlich model.

Table S6. RhB maximum absorption capacities and BET surface area of PAF-215 and other porous adsorbents.

Samples	BET (m^2 g^{-1})	q_m (mg g^{-1})	References
CaPy	28	183	[3]
COF-Z2	549.44	430	[18]
rGO-PDA/ZIF-8	855	688.84	[19]
10%NH_2-ZIF-2 h	999.6	23.955	[4]
DMpillar[5]	1386.7	396.1	[2]
PAF-215	580	1070	This Work

Table S7. MB maximum absorption capacities and BET surface area of PAF-215 and other porous adsorbents.

Samples	BET ($m^2 g^{-1}$)	q_m (mg g^{-1})	References
COPOH+CO	5.2	813	[20]
MAPCTS	28.31	55.68	[21]
CaO-ES@GO	121.14	500	[6]
TzDABA COF	147	315	[7]
Co/C-1000	170.37	805.08	[9]
TdS	257.58	131.59	[22]
SPB-HHTP-DBA	298	884.96	[23]
CTT-POP-2	374	926	[8]
UiO-66$(OH)_2$-Z3	500	203	[24]
UPCH800	1206.95	227.53	[25]
UiO-66-NH_2	1257	309	[26]
KOH/WB-700–2	1522.14	763.94	[27]
KOH/PF-WB-700–2	2301.61	850.34	[27]
PAF-215	580	1020	This Work

Table S8. TC maximum absorption capacities and BET surface area of PAF-215 and other porous adsorbents.

Samples	BET ($m^2 g^{-1}$)	q_m (mg g^{-1})	References
Alg@MOF-rGO	1.61	43.76	[28]
Fe-BTC-HBs	109.03	223.6	[10]
Co_3O_4 QDs-SBE@C	191.11	380.3	[29]
ZIF-67@WA	205.16	273.84	[11]
NMF/TT-90	359	118.48	[13]
TPE-2Py@DSMIL-125(Ti)	516.18	159.2	[30]
CoUiO-1	815.18	224.1	[31]
CM	1058	400	[12]
PAF-215	580	826	This Work

Table S9. CIP maximum absorption capacities and BET surface area of PAF-215 and other porous adsorbents.

Samples	BET (m^2 g^{-1})	q_m (mg g^{-1})	References
LN/MMT@cellulose	1.48	149.6	[32]
FSSi@SA-sula	15.95	365.66	[33]
graphene oxide	90.45	354.24	[34]
COF@MXene	105.73	89.29	[15]
Tb@TpPa-SO_3H	182	956	[16]
ZnCo-ZIF@CS-20	337.25	348.9	[35]
Fe/Ni-MOFs	497.9	232	[36]
Fe-POP	597	13.92	[17]
SMC	1215.48	222.71	[14]
PAF-215	580	1134	This Work

References:

1. J. X. Jiang, F. Su, A. Trewin, C. D. Wood, N. L. Campbell, H. Niu, C. Dickinson, A. Y. Ganin, M. J. Rosseinsky, Y. Z. Khimyak and A. I. Cooper, Conjugated microporous poly (aryleneethynylene) networks, *Angew. Chem.-Int. Edit.*, 2007, **46**, 8574-8578.
2. P. P. Yang, X. J. Hu, Y. Z. Tu, G. Z. Xu, L. Sun and X. C. Xie, The synthesis of a DMpillar 5 arene-based porous polymer with ultrafast adsorption rate and high adsorption capacity for organic micropollutants from water, *Chem. Eng. J.*, 2022, **435**, 11.
3. L. C. Tian, S. Y. Zhou, J. J. Zhao, Q. F. Xu, N. J. Li, D. Y. Chen, H. Li, J. H. He and J. M. Lu, Sulfonate-modified calixarene-based porous organic polymers for electrostatic enhancement and efficient rapid removal of cationic dyes in water, *J. Hazard. Mater.*, 2023, **441**, 13.
4. Z. Huang, J. Rath, Q. C. Zhou, A. Cherevan, S. Naghdi and D. Eder, Hierarchically Micro- and Mesoporous Zeolitic Imidazolate Frameworks Through Selective Ligand Removal, *Small*, 2024, **20**, 11.
5. N. Li, L. L. Huo, W. J. Shen, C. H. Qiang, M. M. Wu, G. F. Sun, Q. F. Li, M. H. Shi and J. Q. Ma, Porous organic polymers for superefficient removal of pollutants from water: Design, synthesis and adsorption performance, *J. Cleaner Prod.*, 2023, **396**, 9.
6. K. S. Obayomi, S. Y. Lau, M. K. Danquah, J. H. Zhang, T. Chiong, O. V. Obayomi, L. Meunier and M. M. Rahman, A response surface methodology approach for the removal of methylene blue dye from wastewater using sustainable and cost-effective adsorbent, *Process Saf. Environ. Protect.*, 2024, **184**, 129-150.
7. R. Li, K. Zhang, X. Yang, R. Xiao, Y. Xie, X. H. Tang, G. Miao, J. Fan, W. G. Zhang, S. R. Zheng and S. L. Cai, Construction of a carboxyl-functionalized clover-like covalent organic framework for selective adsorption of organic dyes, *Sep. Purif. Technol.*, 2024, **340**, 10.
8. Y. Zhang, X. Hong, X. M. Cao, X. Q. Huang, B. Hu, S. Y. Ding and H. Lin, Functional Porous Organic Polymers with Conjugated Triaryl Triazine as the Core for Superfast Adsorption Removal of Organic Dyes, *ACS Appl. Mater. Interfaces*, 2021, **13**, 6359-6366.
9. X. F. Ma, S. Y. Zhao, Z. W. Tian, G. G. Duan, H. Y. Pan, Y. Y. Yue, S. S. Li, S. J. Jian, W. S. Yang, K. M. Liu, S. J. He and S. H. Jiang, MOFs meet wood: Reusable magnetic hydrophilic composites toward efficient water treatment with super-high dye adsorption capacity at high dye concentration, *Chem. Eng. J.*, 2022, **446**, 9.
10. C. F. Zheng, Q. Wu, X. J. Hu, J. X. Ma, K. Y. Sun, Y. J. Sun and B. C. Xu, Macro-manufacturing robust and stable metal-organic framework beads for antibiotics removal from wastewater, *Environ. Res.*, 2024, **246**, 13.
11. G. Y. Chen, S. He, G. B. Shi, Y. S. Ma, C. C. Ruan, X. Jin, Q. L. Chen, X. Y. Liu, H. M. Dai, X. F. Chen and D. M. Huang, In-situ immobilization of ZIF-67 on wood aerogel for effective removal of tetracycline from water, *Chem. Eng. J.*, 2021, **423**, 12.
12. W. Sebai, S. Ahmad, N. Brun, T. Cacciaguerra, D. Cot, A. Boccheciampe, P. Chaurand, C. Levard, M. P. Belleville, J. Sanchez-Marcano and A. Galarneau, Treatment of Wastewater Containing Pharmaceutical Micropollutants by Adsorption under Flow in Highly Porous Carbon Monoliths, *Chem. Mater.*, 2023, **35**, 8464-8482.
13. N. Yuan, C. Zhang, X. L. Zhang and R. H. Zhang, Covalent integration of Fe-based metal-organic framework and triazine-containing covalent organic framework for enhanced adsorptive removal of antibiotics, *J. Cleaner Prod.*, 2024, **434**, 10.
14. B. Wang, Q. Y. Mo, B. Qin, L. Song, J. Li, G. S. Sheng, D. Z. Shi, X. Y. Xu and L. A. Hou, Adsorption behaviors of three antibiotics in single and co-existing aqueous solutions using mesoporous carbon, *Environ. Res.*, 2022, **215**, 12.
15. Y. L. Yang, Q. Y. Liu, Y. M. Zou, M. Tian, L. C. Wang, L. L. Li, M. Y. Wang, Y. Q. Tao, J. J. Wang, Z. Wen, F. M. Ke, D. D. Wang and D. Gao, Covalent assembly synthesis of covalent organic framework and MXene

based composite for the adsorption of fluoroquinolones, *J. Environ. Chem. Eng.*, 2023, **11**, 15.

16. W. Jiang, W. R. Cui, R. P. Liang and J. D. Qiu, Difunctional covalent organic framework hybrid material for synergistic adsorption and selective removal of fluoroquinolone antibiotics, *J. Hazard. Mater.*, 2021, **413**, 9.
17. S. M. Khaledi, M. Taherimehr and S. K. Hassaninejad-Darzi, Porous Fe-Porphyrin as an Efficient Adsorbent for the Removal of Ciprofloxacin from Water, *ACS Omega*, 2024, **9**, 15950-15958.
18. J. Zhao, X. Y. Shen, Y. F. Liu and R. Y. Zou, (3,3)-Connected Triazine-Based Covalent Organic Frameworks for Efficient CO_2 Separation over N_2 and Dye Adsorption, *Langmuir*, 2023, **39**, 16367-16373.
19. N. A. Mazlan, F. S. Butt, A. Lewis, R. Krishnamoorthi, S. Y. Chen, N. Radacsi and Y. Huang, Robust reduced graphene oxide-PDA/ZIF-8 aerogel composite for cyclic, high-capacity dye adsorption, *Sep. Purif. Technol.*, 2024, **334**, 15.
20. D. X. Cao, Y. Chen, W. L. Jin, W. Li, R. Wang, K. Wang, A. N. Tang, L. N. Zhu and D. M. Kong, Non-porous covalent organic polymers enable ultrafast removal of cationic dyes via carbonyl/hydroxyl-synergetic electrostatic adsorption, *Sep. Purif. Technol.*, 2023, **315**, 10.
21. L. J. Ji, L. P. Luo, D. Jin and X. Qin, Preparation of aligned porous carbon microtubes by a reactant permeation template method and the highly selective adsorption of methylene blue dye from wastewater, *Sep. Purif. Technol.*, 2024, **332**, 10.
22. P. D. Sarvalkar, A. S. Vadanagekar, O. S. Karvekar, P. D. Kumbhar, S. S. Terdale, A. S. Thounaojam, S. S. Kolekar, R. S. Vhatkar, P. S. Patil and K. K. K. Sharma, Thermodynamics of Azo Dye Adsorption on a Newly Synthesized Titania-Doped Silica Aerogel by Cogelation: A Comparative Investigation with Silica Aerogels and Activated Charcoal, *ACS Omega*, 2023, **8**, 13285-13299.
23. S. Xue, Q. Wei, R. Zhang, T. Y. Zhang, G. G. Duan, X. S. Han, K. M. Liu, J. Q. Han, S. J. He and S. H. Jiang, Spiroborate-based three dimensional covalent organic framework for effective adsorption and separation of organic dyes, *Sep. Purif. Technol.*, 2024, **341**, 11.
24. P. Damacet, K. Hannouche, A. Gouda and M. Hmadeh, Controlled Growth of Highly Defected Zirconium-Metal-Organic Frameworks via a Reaction-Diffusion System for Water Remediation, *ACS Appl. Mater. Interfaces*, 2024, DOI: 10.1021/acsami.3c16327, 10.
25. X. Y. Yuan, X. Y. Wang, S. Q. Hu, S. Q. Sun and C. L. Li, PDA@UiO-66-NH 2-derived nitrogen and oxygen-doped hierarchical porous carbon for efficient adsorption of BPA and dyes, *Sep. Purif. Technol.*, 2024, **343**, 10.
26. A. Hani, R. R. Haikal, W. A. El-Mehalmey, Y. Safwat and M. H. Alkordi, Durable and recyclable MOF@polycaprolactone mixed-matrix membranes with hierarchical porosity for wastewater treatment, *Nanoscale*, 2023, **15**, 19617-19628.
27. Z. X. Zhang, M. C. Zhang, X. Q. Zhao and J. Z. Cao, High-efficient removal and adsorption mechanism of organic dyes in wastewater by KOH-activated biochar from phenol-formaldehyde resin modified wood, *Sep. Purif. Technol.*, 2024, **330**, 14.
28. N. Kim, B. Cha, Y. Yea, L. K. Njaramba, S. Vigneshwaran, S. S. D. Elanchezhiyan and C. M. Park, Effective sequestration of tetracycline and ciprofloxacin from aqueous solutions by Al-based metal organic framework and reduced graphene oxide immobilized alginate biosorbents, *Chem. Eng. J.*, 2022, **450**, 14.
29. N. Zhao, Q. Y. Ma, B. F. Zhang, Y. F. Wei, D. Liu, M. Y. Li, H. Y. Li and P. Yuan, Intensive adsorption of tetracycline by cobalt oxide quantum dots-loaded mineral carbon, *Bioresour. Technol.*, 2023, **385**, 10.
30. X. L. Song, J. L. He, Y. Wang, J. L. Wang and S. W. Zhang, A novel MIL-125(Ti)-based nanocomposite for enhanced adsorption and catalytic degradation of tetracycline hydrochloride: Synergetic mechanism of calcination and the nitrogen-containing reticulated surface layer, *J. Colloid Interface Sci.*, 2023, **645**, 918-932.
31. J. Cao, Z. H. Yang, W. P. Xiong, Y. Y. Zhou, Y. R. Peng, X. Li, C. Y. Zhou, R. Xu and Y. R. Zhang, One-step

synthesis of Co-doped UiO-66 nanoparticle with enhanced removal efficiency of tetracycline: Simultaneous adsorption and photocatalysis, *Chem. Eng. J.*, 2018, **353**, 126-137.

32. N. Li, K. K. Tao, W. Xia, C. W. Yu and H. Yang, A novel cellulose/lignin/montmorillonite ternary hybrid aerogel for efficiently adsorptive removal of antibiotics from water, *Chem. Eng. J.*, 2023, **466**, 12.
33. J. Y. Jiang, X. C. Jiang, Y. H. Zou, J. Zhai, W. Ding, H. Li and H. L. Zheng, Facile synthesis of acid catalyzed sulfonic acid-amide functionalized magnetic sodium alginate and its efficient adsorption for ciprofloxacin and moxifloxacin, *J. Cleaner Prod.*, 2023, **391**, 11.
34. F. D. Bruckmann, A. Fuhr, L. Zibetti, C. R. Bender, L. F. O. Silva, K. D. Martinello, N. Ahmad, S. Mohandoss and G. L. Dotto, Adsorption of ciprofloxacin from aqueous solution and fresh synthetic urine by graphene oxide: Conventional and statistical physics modeling approaches, *Chem. Eng. J.*, 2024, **487**, 12.
35. Q. F. Luo, P. P. Liu, L. L. Bi, L. Shi, J. R. Zhou, F. Fang, Q. K. Lv, H. Q. Fu, X. D. Li and J. Li, Selective and efficient removal of ciprofloxacin from water by bimetallic MOF beads: Mechanism quantitative analysis and dynamic adsorption, *Sep. Purif. Technol.*, 2024, **332**, 11.
36. F. H. Wei, K. Wang, W. X. Li, Q. H. Ren, L. Qin, M. J. Yu, Z. Liang, M. Nie and S. Y. Wang, Preparation of Fe/Ni-MOFs for the Adsorption of Ciprofloxacin from Wastewater, *Molecules*, 2023, **28**, 17.